MODIFIED FUZZY SPEED CONTROLLER OF INDUCTION MOTOR DRIVE USING EXTENDED KALMAN FILTERING

DUNG Q. NGUYEN[1], HAU H. VO[1], PAVEL BRANDSTETTER[2]

[1]Modeling Evolutionary Algorithms Simulation and Artificial Intelligence, Faculty of Electrical and Electronics Engineering, Ton Duc Thang University, No. 19 Nguyen Huu Tho Street, Tan Phong Ward, District 7, Ho Chi Minh City, Vietnam

[2]Department of Applied Electronics, Faculty of Electrical Engineering and Computer Science, VSB-Technical University of Ostrava, 17. listopadu 15, 708 00 Ostrava, Czech Republic

DOI: 10.17973/MMSJ.2024_12_2024047

vohuuhau@tdtu.edu.vn

This paper focuses on application of fuzzy logic to enhance induction motor drive performance in case where the measured stator currents are distorted by Gaussian noise. For different load torques, the fixed proportional-integral (PI) speed controller provides an undesired drive performance for both transient and steady-state responses. At first, load torque is computed thanks to extended-Kalman-filtered stator currents. Next, load magnitude is employed to adjust the proportional gain and integral constant time of the fuzzy logic (FL) proportional-integral (PI) speed controller. Simulations of drive using two controllers: FL-PI and fixed PI ones, are carried out in different cases of stator current noise and load variation. Performance evaluations indicate that the FL-PI speed controller reduces the assessed indices and increases robustness to noise and load variation.

KEYWORDS

induction motor drive, proportional-integral controller, extended Kalman filter, load torque, fuzzy logic

LIST OF ABBREVIATIONS

DTC	direct torque control
EKF	extended KF
FBR	forward braking
FL	fuzzy logic
FMO	forward motoring
FPC	fuzzy-logic PI speed controller
IM	induction motor
KF	Kalman filtering
MKF	IM-state-space-model-based EKF
PC	fixed PI speed controller
PI	proportional-integral
RBR	reverse braking
RMO	reverse motoring
SC	Signal Computation
STA	starting
SVM	space vector modulation
ULO	unloading

1 INTRODUCTION

Kalman filtering (KF) methods have been widely used to estimate the states or parameters of dynamical systems, such as induction motor (IM) drive systems [Auger et al. 2013, Bose 2002]. The stator current and its time derivative are obtained using the non-IM-model-based KF for a sensorless IM drive [Brandstetter et al. 2017]. The extended KF (EKF) was associated with current derivative measurements for state and parameter estimation in synchronous reluctance motor drive [Mynar et al. 2021]. An adaptive KF technique was used to estimate the torque precisely [Stender et al. 2021].

Along with intelligent methods such as genetic algorithms and neural networks [Aissa et al. 2024, Tran et al. 2017], fuzzy logic (FL) has been widely used in engineering. The active power filter was controlled by the FL [Djendaoui et al. 2021]. To reduce the horizontal vibration of an elevator car system, the FL was combined with sliding mode control [Ge et al. 2023]. A type-2 FL system was presented to deal with rule uncertainties [Karnik et al. 1999]. To increase the reliability of the failure mode and effect analysis, the FL was integrated [Laufer 2024]. To optimize the distribution system network reconfiguration for electric vehicles, the FL was employed [Mohanty 2023]. Type-2 FL controllers were compared for their robustness to noise [Ontiveros-Robles et al. 2018]. The combination of the FL and neural network was used for diagnosis of devices such as electric drives and bearings in mechatronic systems [Peterka 2020].

In electrical drives, various FL techniques have been utilized to improve performance of fault detection, observer, controller, identification. An FL classifier was utilized to detect stator-winding faults in cage IMs [Aswad et al. 2023]. An adaptation mechanism was combined with a type-2 FL controller to ensure robustness to parameter changes at low speeds [Benlaloui et al. 2019]. Motor speed and torque were estimated by the FL-based observer [Fedor et al. 2023]. The FL systems were utilized to resolve stochastic functions in the IM drive systems [Kang et al. 2022]. Sensorless control using model reference adaptive system for permanent magnet synchronous motor (PMSM) drive was enhanced by the FL [Khanh 2022]. An adaptive FL control scheme was applied to an IM drive under load variations and disturbance [Ma et al. 2023]. The drive of a multi-motor system was implemented using state-space-representation-based fuzzy model [Perdukova 2023]. The boundaries of integral time constant were adjusted to reduce the undershoot and overshoot in a proportional-integral (PI) based FL speed controller [Vo 2023b]. However, the method was based on function of speed error with coefficient tuned by trial-and-error technique. Next, the KF uses the state-space representation to obtain filtered stator currents in the case of known measurement noise. Then, the filtered currents are employed to calculate important quantities for space vector modulation-direct torque control (SVM-DTC). Finally, the calculated load torque is used to adjust boundaries of both integral time constant and proportional gain. The section structure of the paper is organized as follows: Introduction – Proposed Induction Motor Drive Structure – Simulations and Discussions – Conclusions.

2 PROPOSED INDUCTION MOTOR DRIVE STRUCTURE

Figure 1 shows the proposed structure using a fuzzy-logic PI speed controller (FPC) with IM-state-space-model-based extended Kalman filtering (MKF) for the SVM-direct torque controlled drive. The state-space representation of the IM is described as Eqs. (1)-(2) (Bose 2002):

$$\frac{dX}{dt} = \mathbf{AX} + \mathbf{B}U \tag{1}$$

$$\boldsymbol{Y} = \mathbf{C}\boldsymbol{X} \tag{2}$$

where $\mathbf{A}$, $\mathbf{B}$, and $\mathbf{C}$: system, input, and output matrices; $\boldsymbol{X}$, $\boldsymbol{U}$, and $\boldsymbol{Y}$: state, input, and output vectors. The matrices and vectors are expressed by Eqs. (3)-(8):

$$\mathbf{A} = \begin{bmatrix} a_1 & 0 & a_2 & a_3\omega_m \\ 0 & a_1 & -a_3\omega_m & a_2 \\ \frac{L_m R_r}{L_r} & 0 & -\frac{R_r}{L_r} & -n_p\omega_m \\ 0 & \frac{L_m R_r}{L_r} & n_p\omega_m & -\frac{R_r}{L_r} \end{bmatrix} \tag{3}$$

$$\mathbf{B} = \begin{bmatrix} \frac{1}{\sigma L_s} & 0 & 0 & 0 \\ 0 & \frac{1}{\sigma L_s} & 0 & 0 \end{bmatrix}^T \tag{4}$$

$$\mathbf{C} = \begin{bmatrix} 1 & 0 & 0 & 0 \\ 0 & 1 & 0 & 0 \end{bmatrix} \tag{5}$$

$$\boldsymbol{X} = \begin{bmatrix} i_{s\alpha} & i_{s\beta} & \psi_{r\alpha} & \psi_{r\beta} \end{bmatrix}^T \tag{6}$$

$$\boldsymbol{U} = \begin{bmatrix} u_{s\alpha} & u_{s\beta} \end{bmatrix}^T \tag{7}$$

$$\boldsymbol{Y} = \begin{bmatrix} i_{s\alpha} & i_{s\beta} \end{bmatrix}^T \tag{8}$$

where: ω_m: mechanical speed; n_p: number of pole pairs; L_m, L_s, and L_r: magnetizing, stator, and rotor inductances; R_s and R_r: stator and rotor resistances; $i_{s\alpha}$ & $i_{s\beta}$, $u_{s\alpha}$ & $u_{s\beta}$, and $\psi_{r\alpha}$ & $\psi_{r\beta}$ two components α- & β- of stator current, stator voltage, and rotor flux vectors in stator reference frame. The coefficients a_1, a_2, a_3, and σ are calculated according to Eqs. (9)-(12):

$$a_1 = -\frac{L_m^2 R_r + L_r^2 R_s}{\sigma L_s L_r^2} \tag{9}$$

$$a_2 = \frac{L_m R_r}{\sigma L_s L_r^2} \tag{10}$$

$$a_3 = \frac{n_p L_m}{\sigma L_s L_r} \tag{11}$$

$$\sigma = 1 - \frac{L_m^2}{L_s L_r} \tag{12}$$

The system described by Eqs. (1)-(2), is discretized by the Euler method. Assume that the discretized system is distorted by zero-mean, Gaussian process & measurement noise vectors $\boldsymbol{v}$ & $\boldsymbol{w}$ as Eqs. (13)-(14):

$$\boldsymbol{X}(k+1) = \mathbf{A}_d \boldsymbol{X}(k) + \mathbf{B}_d \boldsymbol{U}(k) + \boldsymbol{v}(k) \tag{13}$$

$$\boldsymbol{Y}(k) = \mathbf{C}_d \boldsymbol{X}(k) + \boldsymbol{w}(k) \tag{14}$$

where t_d : discretization period; $\mathbf{A}_d$, $\mathbf{B}_d$, and $\mathbf{C}_d$: system, input, and output matrices of the discretized system are computed according to Eqs. (15)-(17):

$$\mathbf{A}_d = \mathbf{I} + t_d \mathbf{A} \tag{15}$$

$$\mathbf{B}_d = t_d \mathbf{B} \tag{16}$$

$$\mathbf{C}_d = \mathbf{C} \tag{17}$$

Utilizing the discretized state-space representation of the IM, the MKF block computes the filtered stator currents $i_{s\alpha,kf}$ and $i_{s\beta,kf}$ according to (18) – (24) (Auger et al. 2013):

$$\tilde{\boldsymbol{X}}(k+1) = \mathbf{A}_d \boldsymbol{X}_{kf}(k) + \mathbf{B}_d \boldsymbol{U}(k) \tag{18}$$

$$\tilde{\mathbf{P}}(k+1) = \mathbf{A}_d(k)\hat{\mathbf{P}}(k)\mathbf{A}_d^T(k) + \mathbf{Q} \tag{19}$$

$$\mathbf{K}(k+1) = \tilde{\mathbf{P}}(k+1)\mathbf{C}_d^T \left[\mathbf{C}_d \tilde{\mathbf{P}}(k+1)\mathbf{C}_d^T + \mathbf{R} \right]^{-1} \tag{20}$$

$$\boldsymbol{X}_{kf}(k+1) = \tilde{\boldsymbol{X}}(k+1) + \mathbf{K}(k+1)\left[\boldsymbol{Y}(k) - \tilde{\boldsymbol{Y}}(k+1) \right] \tag{21}$$

$$\hat{\mathbf{P}}(k+1) = \tilde{\mathbf{P}}(k+1) - \mathbf{K}(k+1)\mathbf{C}_d \tilde{\mathbf{P}}(k+1) \tag{22}$$

$$\boldsymbol{Y}(k) = \mathbf{C}_d \boldsymbol{X}(k) \tag{23}$$

$$\tilde{\boldsymbol{Y}}(k) = \mathbf{C}_d \tilde{\boldsymbol{X}}(k) \tag{24}$$

where: $\mathbf{P}$: state vector covariance matrix; $\mathbf{K}$: Kalman gain matrix; $\mathbf{Q}$ & $\mathbf{R}$: covariance matrices of the noise vectors $\boldsymbol{v}$ & $\boldsymbol{w}$; symbols "~" and "^" denote predicted and estimated quantities, respectively; subscript letters "*kf*" represent Kalman-filtered ones as follows:

$$\boldsymbol{X}_{kf} = \begin{bmatrix} i_{s\alpha,kf} & i_{s\beta,kf} & \psi_{r\alpha,kf} & \psi_{r\beta,kf} \end{bmatrix}^T \tag{25}$$

The filtered stator currents are employed by the Signal Computation (SC) block to obtain essential quantities for the blocks: flux & torque controllers, vector rotation, and the FPC, according to Eqs. (26)-(31):

$$\frac{d\psi_{s\alpha,c}}{dt} = u_{s\alpha} - R_s i_{s\alpha,kf} \tag{26}$$

$$\frac{d\psi_{s\beta,c}}{dt} = u_{s\beta} - R_s i_{s\beta,kf} \tag{27}$$

$$\psi_{s,c} = \sqrt{\psi_{s\alpha,c}^2 + \psi_{s\beta,c}^2} \tag{28}$$

$$T_{e,c} = 1.5 n_p \left(\psi_{s\alpha,c} i_{s\beta,kf} - \psi_{s\beta,c} i_{s\alpha,kf} \right) \tag{29}$$

$$\gamma_c = \sin^{-1}\left(\frac{\psi_{s\beta,c}}{\psi_{s,c}} \right) \tag{30}$$

$$T_{l,c} = T_{e,c} - J_m \frac{d\omega_m}{dt} - B_m \omega_m \tag{31}$$

where: J_m – motor inertia; B_m – rotational damping constant; subscript letter "*c*" presents corresponding values that are computed by the SC block including stator flux components $\psi_{s\alpha}$ & $\psi_{s\beta}$, stator flux magnitude ψ_s, electromagnetic torque T_e, orienting angle γ, and load torque T_l.

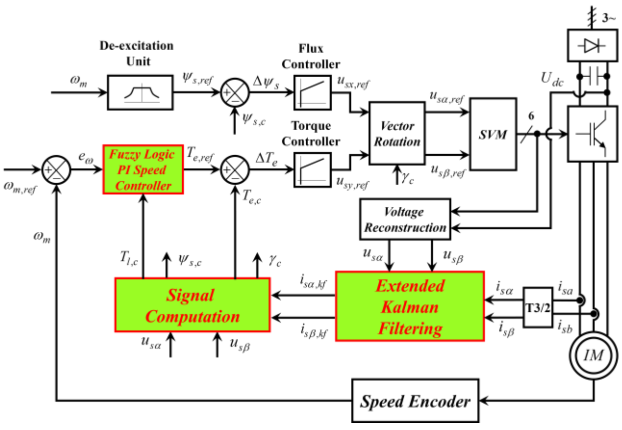

Figure 1. The proposed IM drive structure

The FPC block shown in Fig. 2 updates the proportional gain and integral time constant according to three following steps: fuzzification, fuzzy rule base and inference engine making, and defuzzification. The two inputs of the fuzzification are the speed error e_ω and its difference, Δe_ω. The three linguistic variables, P, Z, N of the inputs denote positive, zero, and negative values, respectively, whose membership functions are described by Eqs. (32)-(37):

$$\mu_P(e_\omega)=\begin{cases}1, & e_\omega \ge H_{e_\omega}\\ \dfrac{e_\omega}{H_{e_\omega}}, & 0\le e_\omega < H_{e_\omega}\\ 0, & e_\omega<0\end{cases} \tag{32}$$

$$\mu_Z(e_\omega)=\begin{cases}0, & e_\omega \ge H_{e_\omega}\\ \dfrac{H_{e_\omega}-e_\omega}{H_{e_\omega}}, & 0\le e_\omega < H_{e_\omega}\\ \dfrac{H_{e_\omega}+e_\omega}{H_{e_\omega}}, & -H_{e_\omega}\le e_\omega<0\\ 0, & e_\omega<-H_{e_\omega}\end{cases} \tag{33}$$

$$\mu_N(e_\omega)=\begin{cases}0, & e_\omega \ge 0\\ -\dfrac{e_\omega}{H_{e_\omega}}, & -H_{e_\omega}\le e_\omega < 0\\ 1, & e_\omega<-H_{e_\omega}\end{cases} \tag{34}$$

$$\mu_P(\Delta e_\omega)=\begin{cases}1, & \Delta e_\omega \ge H_{\Delta e_\omega}\\ \dfrac{\Delta e_\omega}{H_{\Delta e_\omega}}, & 0\le \Delta e_\omega < H_{\Delta e_\omega}\\ 0, & \Delta e_\omega<0\end{cases} \tag{35}$$

$$\mu_Z(\Delta e_\omega)=\begin{cases}0, & \Delta e_\omega \ge H_{\Delta e_\omega}\\ \dfrac{H_{\Delta e_\omega}-\Delta e_\omega}{H_{\Delta e_\omega}}, & 0\le \Delta e_\omega < H_{\Delta e_\omega}\\ \dfrac{H_{\Delta e_\omega}+\Delta e_\omega}{H_{\Delta e_\omega}}, & -H_{\Delta e_\omega}\le \Delta e_\omega<0\\ 0, & \Delta e_\omega<-H_{\Delta e_\omega}\end{cases} \tag{36}$$

$$\mu_N(\Delta e_\omega)=\begin{cases}0, & \Delta e_\omega \ge 0\\ -\dfrac{\Delta e_\omega}{H_{\Delta e_\omega}}, & -H_{\Delta e_\omega}\le \Delta e_\omega < 0\\ 1, & \Delta e_\omega<-H_{\Delta e_\omega}\end{cases} \tag{37}$$

where $H_{e\omega} > 0$ and $H_{\Delta e\omega} > 0$. The large, medium, and small values of three linguistic variables L, M, S for two outputs, proportional gain K_p and inverse of integral time constant T_i of the defuzzification, are derived by the fuzzy rule base and inference engine shown in Tab. 1. Membership functions for L, M, S are expressed by Eqs. (38)-(43), respectively:

$$\mu_L(K_p)=\begin{cases}1, & K_p\ge h_p\\ \dfrac{K_p-cen_p}{h_p-cen_p}, & cen_p<K_p<h_p\\ 0, & K_p\le cen_p\end{cases} \tag{38}$$

$$\mu_M(K_p)=\begin{cases}0, & K_p\le l_p\\ \dfrac{K_p-l_p}{cen_p-l_p}, & l_p<K_p<cen_p\\ \dfrac{h_p-K_p}{h_p-cen_p}, & cen_p\le K_p<h_p\\ 0, & K_p\ge h_p\end{cases} \tag{39}$$

$$\mu_S(K_p)=\begin{cases}1, & K_p\le l_p\\ \dfrac{cen_p-K_p}{cen_p-l_p}, & l_p<K_p<cen_p\\ 0, & K_p\ge cen_p\end{cases} \tag{40}$$

$$\mu_L(T_i^{-1})=\begin{cases}1, & T_i^{-1}\ge h_i\\ \dfrac{T_i^{-1}-cen_i}{h_i-cen_i}, & cen_i<T_i^{-1}<h_i\\ 0, & T_i^{-1}\le cen_i\end{cases} \tag{41}$$

$$\mu_M(T_i^{-1})=\begin{cases}0, & T_i^{-1}\le l_i\\ \dfrac{T_i^{-1}-l_i}{cen_i-l_i}, l_i<T_i^{-1}<cen_i & \\ \dfrac{h_i-T_i^{-1}}{h_i-cen_i}, & cen_i\le T_i^{-1}<h_i\\ 0, & T_i^{-1}\ge h_i\end{cases} \tag{42}$$

$$\mu_S(T_i^{-1})=\begin{cases}1, & T_i^{-1}\le l_i\\ \dfrac{cen_i-T_i^{-1}}{cen_i-l_i}, & l_i<T_i^{-1}<cen_i\\ 0, & T_i^{-1}\ge cen_i\end{cases} \tag{43}$$

where: boundaries of the proportional gain h_p & l_p and the integral time constant h_i & l_i depend on cen_p & b_p and cen_i & b_i according to Eqs. (44)-(45) and Eqs. (46)-(47), respectively:

$$h_p=cen_p+b_p \tag{44}$$

$$l_p=cen_p-b_p \tag{45}$$

$$h_i=\frac{1}{cen_i^{-1}-b_i} \tag{46}$$

$$l_i=\frac{1}{cen_i^{-1}+b_i} \tag{47}$$

where: $0 < b_p < cen_p$; $0 < b_i < (cen_i)^{-1}$. The defuzzification block employs the centroid method to compute crisp values of the outputs. The magnitude of the computed load torque is limited to the range $[-0.7T_n, 0.7T_n]$ where T_n is the rated torque. The limited value is normalized to the range $[0, 0.7T_n]$ to obtain parameter $T_{l,n}$. The normalized value $T_{l,n}$ is discretized using Eq. (48):

$$q = \lfloor 5T_{l,n} \rfloor + 1 \quad (48)$$

where q is an integer ranging from one to six. The parameter q is utilized to adjust the parameters of the FPC according to Eqs. (49)-(52):

$$cen_p = \frac{q+12}{10} K_{p,\mathrm{PC}} \quad (49)$$

$$b_p = \frac{q+2}{20} K_{p,\mathrm{PC}} \quad (50)$$

$$cen_i^{-1} = \frac{8-q}{10} T_{i,\mathrm{PC}} \quad (51)$$

$$b_i = \frac{cen_i^{-1}}{10} \quad (52)$$

With this parameter update, the FPC can be considered a discontinuous type-2 fuzzy system. Parameters surfaces of the FPC in cases of q = 1, and q = 6 are shown in Figs. 3-4. The axes of variables e_ω and Δe_ω in the figures are divided by $\omega_{m,ref}$.

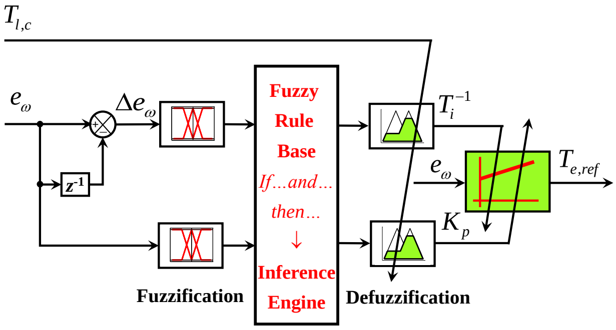

Figure 2. Fuzzy logic PI speed controller

Δe_ω	e_ω		
	P	**Z**	**N**
P	L, S	M, S	S, S
Z	L, M	M, M	S, M
N	L, L	M, L	S, L

Table 1. Fuzzy rule base and inference engine

3 SIMULATIONS AND DISCUSSIONS

Drives utilizing two speed controllers, fixed PI speed controller (PC) and the FPC, are implemented in Matlab/Simulink environment at reference mechanical speeds of π (rad/s) and 10π (rad/s), load torques of $0.1T_n$ and $0.7T_n$, and variance δ^2 of stator current measurement noise of 0.25^2 and 1.0^2. Tables 2 and 3 show the parameters of the IM and drive, respectively. In time courses, there are 6 durations: 0.0s-0.5s, 0.5s-0.9s, 0.9s-1.3s, 1.3s-2.4s, 2.4s-2.7s, and 2.7s-3.0s, corresponding to 6 operations of the IM drive including starting (STA), forward motoring (FMO), forward braking (FBR), reverse motoring (RMO), reverse braking (RBR), and unloading (ULO) [Vo 2023a].

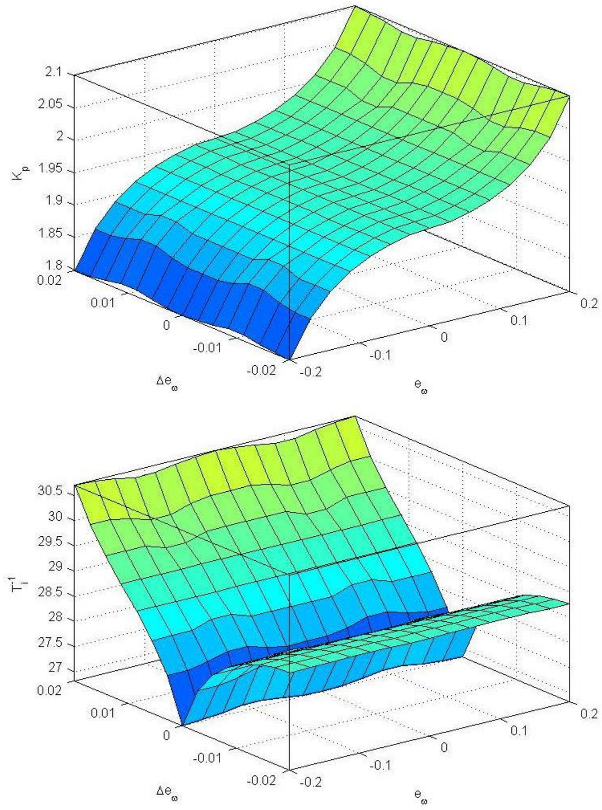

Figure 3. Parameters surface of the FPC: K_p (upper) and T_i^{-1}, case q = 1

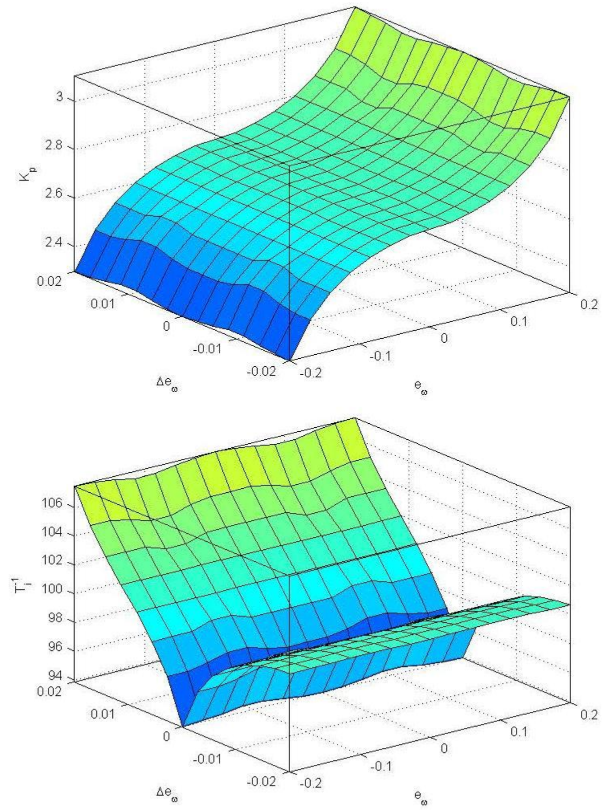

Figure 4. Parameters surface of the FPC: K_p (upper) and T_i^{-1}, case q = 6

Parameter	Value	Parameter	Value
Rated power	2.2kW	Motor inertia	0.0047kg.m^2
Rated	14N.m	Mutual	0.192H

torque		inductance	
Rated voltage	230V/400V	Stator/rotor inductance	0.209H
Rated speed	1420rpm	Stator resistance	3.179Ω
Number of pole pairs	2	Rotor resistance	2.118Ω

Table 2. The motor parameters [Vo 2023a]

Block	Parameter	Value
Speed controller	Proportional gain $K_{p,PC}$	1.5
	Integral time constant $T_{i,PC}$	0.05s
	Output limits	±14N.m
Flux controller	Proportional gain	100
	Integral time constant	0.01s
Torque controller	Proportional gain	5
	Integral time constant	0.05s
Voltage source inverter	DC link voltage	540V
	Switching frequency	4kHz
	Modulation technique	SVM

Table 3. The drive parameters [Vo 2023a]

Figures 5-12 show mechanical speed responses for listed cases of noise variance, load torque, and reference mechanical speed. Through enlarged images shown in the figures, it is easy to see that the speed response of the FPC has lower overshoot/undershoot than that of the PC. For more detail, overshoot/undershoot is displayed in Tabs. 4-9 corresponding to IM operations. For the starting (see Tab. 4) , the FPC overshoot is reduced by at most 61% compared to the PC one at $\omega_{m,ref} = \pi$, $\delta^2=1^2$. For the FMO, FBR and RBR operations (see Tabs. 5, 6 and 8), the cases where FPC's overshoot decreases the most compared to PC's occur at the highest load torque. Cases of the RMO and ULO operations (see Tabs. 7 and 9), the greatest reduction in FPC overshoot compared to PC overshoot is achieved at maximum load or maximum noise variance. In order to compare the performance at steady state of two speed controllers, the ripple calculated during last 0.1 second of each drive operation, is listed in Tabs. 10-15.

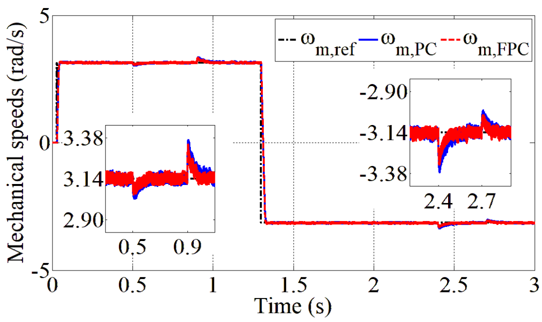

Figure 5. Speeds at $\omega_{m,ref} = \pi$ (rad/s), $T_l = 0.1T_n$, $\delta^2=0.25^2$

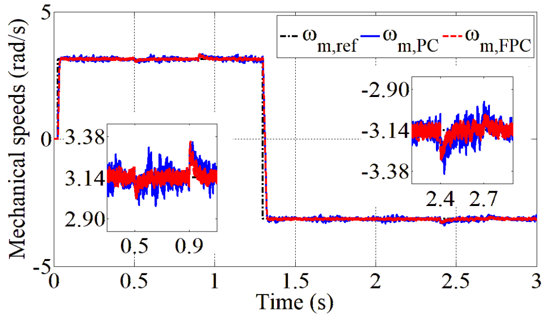

Figure 6. Speeds at $\omega_{m,ref} = \pi$ (rad/s), $T_l = 0.1T_n$, $\delta^2=1.0^2$

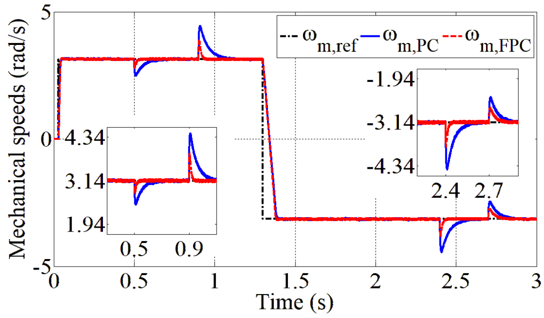

Figure 7. Speeds at $\omega_{m,ref} = \pi$ (rad/s), $T_l = 0.7T_n$, $\delta^2=0.25^2$

In Tab. 10, the ripple for the STA operation of the FPC is decreased by at most 48% compared to that of the PC at $\omega_{m,ref} = 10\pi$, $\delta^2=1^2$. For the five remaining operations (Tabs. 11-15), the FPC ripple is increasingly reduced compared to the PC ripple as the noise variance increases. Figures 13-14 show the speed responses at $\omega_{m,ref} = \{\pi, 10\pi\}$, $T_l = 0.7T_n$, $\delta^2= 2^2$. They indicated that the FPC is much more robust than the PC in the case of large noise variances and the highest load torque. In particular, the PC cannot track the reference signal during the RMO operation (see blue waveform in Fig. 14). The filtered stator current responses at $\omega_{m,ref} = \{\pi, 10\pi\}$, $T_l = 0.7T_n$, $\delta^2= \{1^2, 2^2\}$ are displayed in Figs. 15-18. Although currents are smoothed by the MKF, they tend to deviate from the sine wave shape as the noise variance increases, particularly for the PC. The parameter q shown in Figs. 19-20 indicates that as variance δ^2 increases, the calculated load torque fluctuates.

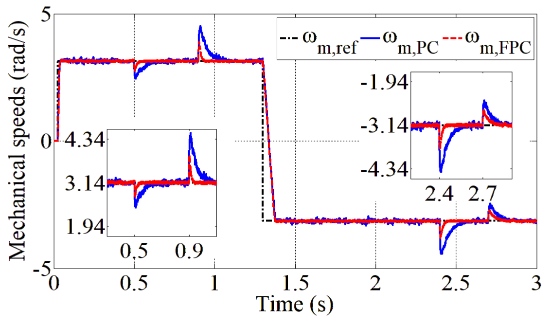

Figure 8. Speeds at $\omega_{m,ref} = \pi$ (rad/s), $T_l = 0.7T_n$, $\delta^2=1.0^2$

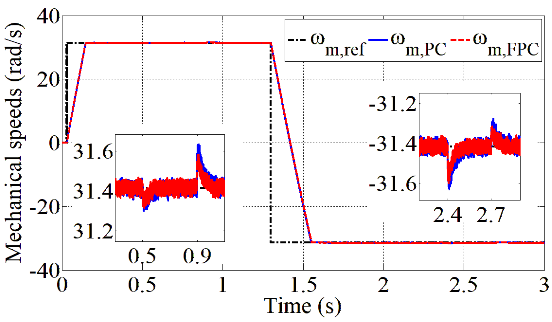

Figure 9. Speeds at $\omega_{m,ref}$ = 10π (rad/s), T_l = 0.1T_n, ϑ=0.25²

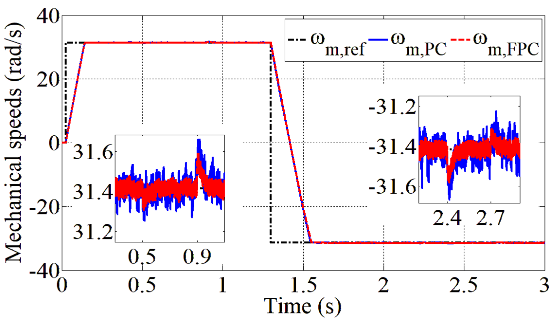

Figure 10. Speeds at $\omega_{m,ref}$ = 10π (rad/s), T_l = 0.1T_n, ϑ=1.0²

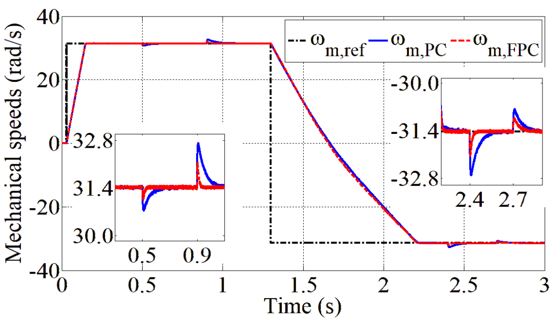

Figure 11. Speeds at $\omega_{m,ref}$ = 10π (rad/s), T_l = 0.7T_n, ϑ=0.25²

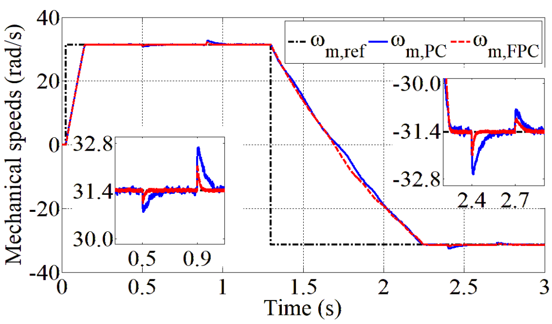

Figure 12. Speeds at $\omega_{m,ref}$ = 10π (rad/s), T_l = 0.7T_n, ϑ=1.0²

$\omega_{m,ref}$	ϑ			
	0.25²		1.0²	
	PC	FPC	PC	FPC
π	1.63	1.76	5.57	2.12
10π	0.16	0.16	0.37	0.20

Table 4. Overshoot (%) at STA operation

$\omega_{m,ref}$	T_l/T_n	ϑ			
		0.25²		1.0²	
		PC	FPC	PC	FPC
π	0.1	3.81	3.05	5.31	4.16
	0.7	21.2	11.2	21.8	12.6
10π	0.1	0.37	0.33	0.51	0.34
	0.7	2.21	1.21	2.03	1.19

Table 5. Undershoot (%) at FMO operation

$\omega_{m,ref}$	T_l/T_n	ϑ			
		0.25²		1.0²	
		PC	FPC	PC	FPC
π	0.1	7.23	6.41	6.65	6.66
	0.7	41.9	24.3	44.0	23.9
10π	0.1	0.69	0.54	0.78	0.56
	0.7	4.14	2.33	4.04	2.31

Table 6. Overshoot (%) at FBR operation

$\omega_{m,ref}$	T_l/T_n	ϑ			
		0.25²		1.0²	
		PC	FPC	PC	FPC
π	0.1	1.87	1.73	5.82	2.17
	0.7	2.14	1.70	6.04	1.88
10π	0.1	0.18	0.16	0.61	0.21
	0.7	0.17	0.17	0.43	0.19

Table 7. Overshoot (%) at RMO operation

$\omega_{m,ref}$	T_l/T_n	ϑ			
		0.25²		1.0²	
		PC	FPC	PC	FPC
π	0.1	7.41	6.00	8.17	5.54
	0.7	41.7	21.7	41.2	21.6
10π	0.1	0.69	0.58	0.80	0.53
	0.7	4.11	2.31	3.96	2.25

Table 8. Overshoot (%) at RBR operation

$\omega_{m,ref}$	T_l/T_n	ϑ			
		0.25²		1.0²	
		PC	FPC	PC	FPC
π	0.1	4.24	3.34	5.42	3.00
	0.7	22.3	13.0	22.1	13.3
10π	0.1	0.44	0.32	0.60	0.33
	0.7	2.10	1.29	2.09	1.26

Table 9. Undershoot (%) at ULO operation

$\omega_{m,ref}$	ϑ			
	0.25²		1.0²	
	PC	FPC	PC	FPC
π	2.72	2.65	3.91	3.88
10π	0.35	0.33	0.75	0.39

Table 10. Ripple (%) at STA operation

$\omega_{m,ref}$	T_l/T_n	ϑ			
		0.25²		1.0²	
		PC	FPC	PC	FPC
π	0.1	2.49	2.75	5.26	3.60

	0.7	3.02	2.82	7.89	2.90
10π	0.1	0.31	0.31	0.93	0.32
	0.7	0.33	0.35	0.87	0.34

Table 11. Ripple (%) at FMO operation

$\omega_{m,ref}$	T_l/T_n	ϑ			
		0.25^2		1.0^2	
		PC	FPC	PC	FPC
π	0.1	2.95	3.44	8.97	3.61
	0.7	3.15	2.73	6.93	3.20
10π	0.1	0.33	0.29	0.84	0.36
	0.7	0.18	0.18	0.50	0.17

Table 12. Ripple (%) at FBR operation

$\omega_{m,ref}$	T_l/T_n	ϑ			
		0.25^2		1.0^2	
		PC	FPC	PC	FPC
π	0.1	3.11	2.74	6.93	3.52
	0.7	3.26	3.05	6.96	2.96
10π	0.1	0.31	0.34	0.55	0.33
	0.7	0.45	0.33	0.95	0.38

Table 13. Ripple (%) at RMO operation

$\omega_{m,ref}$	T_l/T_n	ϑ			
		0.25^2		1.0^2	
		PC	FPC	PC	FPC
π	0.1	2.89	2.79	8.43	4.23
	0.7	2.90	2.98	8.53	2.69
10π	0.1	0.32	0.29	0.84	0.35
	0.7	0.32	0.29	0.64	0.31

Table 14. Ripple (%) at RBR operation

$\omega_{m,ref}$	T_l/T_n	ϑ			
		0.25^2		1.0^2	
		PC	FPC	PC	FPC
π	0.1	3.04	2.74	8.83	3.86
	0.7	2.82	2.88	6.50	3.98
10π	0.1	0.32	0.32	0.71	0.35
	0.7	0.33	0.30	0.70	0.37

Table 15. Ripple (%) at ULO operation

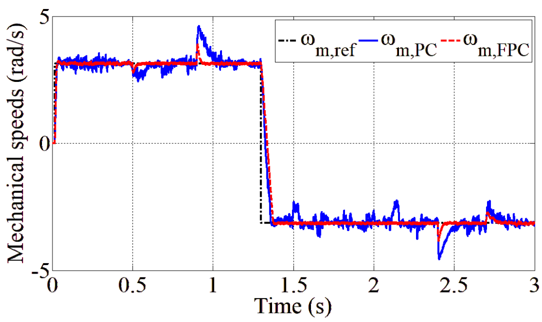

Figure 13. Speeds at $\omega_{m,ref}$ = π (rad/s), T_l = $0.7T_n$, ϑ=2.0^2

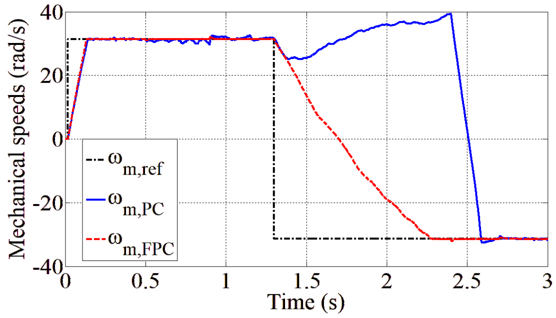

Figure 14. Speeds at $\omega_{m,ref}$ = 10π (rad/s), T_l = $0.7T_n$, ϑ=2.0^2

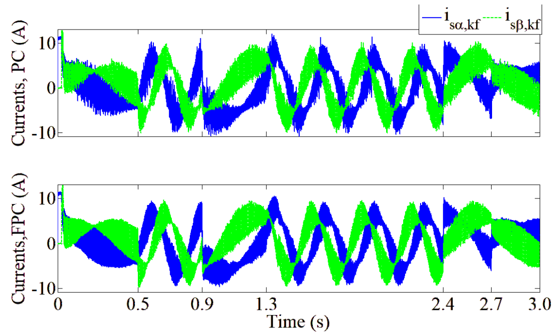

Figure 15. Currents at $\omega_{m,ref}$ = π (rad/s), T_l = $0.7T_n$, ϑ=1.0^2

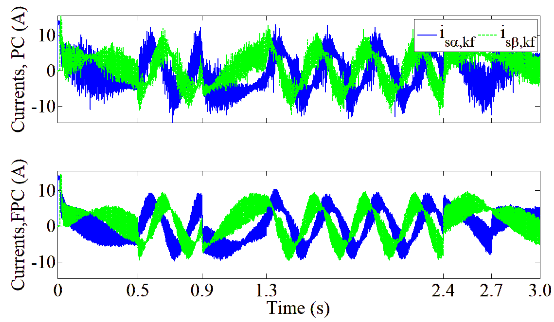

Figure 16. Currents at $\omega_{m,ref}$ = π (rad/s), T_l = $0.7T_n$, ϑ=2.0^2

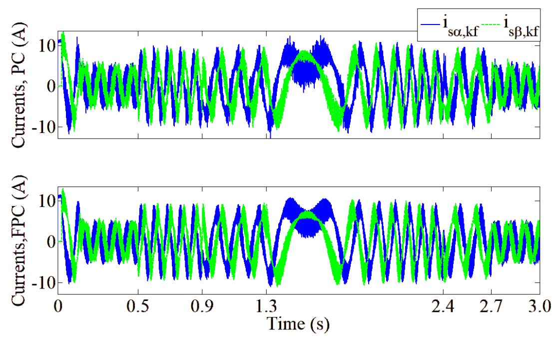

Figure 17. Currents at $\omega_{m,ref}$ = 10π (rad/s), T_l = $0.7T_n$, ϑ=1.0^2

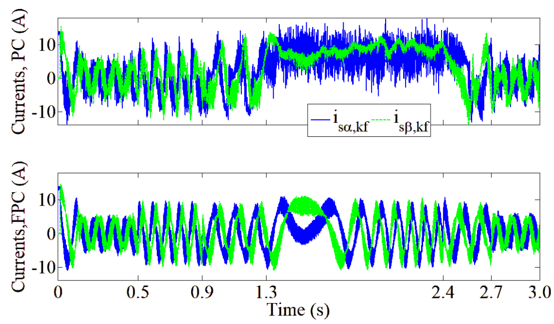

Figure 18. Currents at $\omega_{m,ref}$ = 10π (rad/s), T_l = $0.7T_n$, ϑ=2.0^2

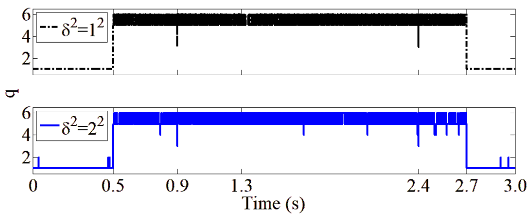

Figure 19. Parameter q at $\omega_{m,ref} = \pi$ (rad/s), $T_l = 0.7T_n$, $\delta^2=\{1.0^2, 2.0^2\}$

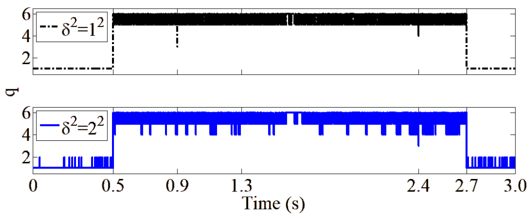

Figure 20. Parameter q at $\omega_{m,ref} = 10\pi$ (rad/s), $T_l = 0.7T_n$, $\delta^2=\{1.0^2, 2.0^2\}$

4 CONCLUSIONS

A drive structure using IM-model-based extended Kalman filtering integrated with a PI speed controller, whose parameters were updated by fuzzy logic according to the computed load torque, was presented. The structure and the one with a fixed-parameter PI speed controller were simulated in different cases of reference mechanical speed, load torque, and known measurement stator current noise covariance. The structure with the FPC significantly improved both the transient and steady-state speed responses compared with the structure with the PC, especially up to 69% and 63% reductions in overshoot/undershoot and ripple at very-low reference mechanical speed and high load torque. In addition, it offered much strong robustness than the one with PC, even in cases of large noise variance. The proposed structure can be used for sensorless IM drives. Adaptive Kalman filtering techniques can be used to obtain more precise information on the load torque magnitude. The FL techniques can be deployed to identify IM parameters. Type-2 or type-3 fuzzy logic can be developed to achieve greater robustness to large variations in disturbance and load torque.

REFERENCES

[Aissa 2024] Aissa, O., et al. Advanced direct torque control based on neural tree controllers for induction motor drives. ISA Transactions, May 2024, Vol.148, pp 92-104. ISSN 0019-0578

[Aswad 2023] Aswad, R. A. K., et al. Hybrid Model-Based Fuzzy Logic Diagnostic System for Stator Faults in Three-Phase Cage Induction Motors. IEEE Access, July 2023, Vol.11, pp 75707-75714. ISSN 2169-3536

[Auger 2013] Auger, F., et al. Industrial Applications of the Kalman Filter: A Review. IEEE Transactions on Industrial Electronics, December 2013, Vol.60, No.12., pp 5458-5471. ISSN 0278-0046

[Benlaloui 2019] Benlaloui, I., et al. MRAS type-2 fuzzy logic observer and controller for robust speed sensorless induction motor. Proceedings of the 2019 International Conference on Control, Automation and Diagnosis (ICCAD), 02-04 July, 2019. Grenoble, France, pp 1-7. ISBN 978-1-7281-2292-2

[Bose 2002] Bose, B. K. Modern Power Electronics and AC Drives. Upper Saddle River, NJ, USA: Prentice Hall, 2002. ISBN 0-13-016743-6

[Brandstetter 2017] Brandstetter, P., et al. Application of BEMF-MRAS with Kalman Filter in Sensorless Control of Induction Motor Drive. Electrical Engineering, December 2017, Vol.99, No.4., pp 1151-1160. ISSN 0948-7921

[Djendaoui 2021] Djendaoui, D., et al. Self Tunning Filter for Three Levels Four Legs Shunt Active Power Filter with Fuzzy Logic Controller. Acta Polytechnica, June 2021, Vol.61, No.3., pp 415-427. ISSN 1210-2709

[Fedor 2023] Fedor, M., et al. Fuzzy Observer of Induction Motor Torque and Speed Based on Dynamic Filters. Proceedings of the 2023 International Conference on Electrical Drives and Power Electronics (EDPE), 25-27 September, 2023. The High Tatras, Slovakia, pp 1-7. ISBN 979-8-3503-2275-0

[Ge 2023] Ge, Q., et al. Study on Fuzzy Sliding Mode Active Disturbance Rejection Control Method for Horizontal Vibration of High-Speed Elevator Car System. Control Engineering and Applied Informatics, June 2023, Vol.25, No.2., pp 13-24. ISSN 1454-8658

[Kang 2022] Kang, S., Liu, P. X. and Wang, H. Finite-time command filter-based adaptive fuzzy tracking control for stochastic nonlinear induction motors systems with unknown backlash-like hysteresis. Journal of the Franklin Institute, October 2022, Vol.359, No.15., pp 7936-7960. ISSN 0016-0032

[Karnik 1999] Karnik, N. N., Mendel, J. M. and Liang, Q. Type-2 fuzzy logic systems. IEEE Transactions on Fuzzy Systems, December 1999, Vol.7, No.6., pp 643-658. ISSN 1063-6706

[Khanh 2022] Khanh, P. Q. and Anh, H. P. H. Novel Sensorless PMSM Speed Control Using Advanced Fuzzy MRAS Algorithm. Arabian Journal for Science and Engineering, November 2022, Vol.47, No.11., pp 14531-14542. ISSN 2191-4281

[Laufer 2024] Laufer, E. Similarity Measure Supported Fuzzy Failure Mode and Effect Analysis. Acta Polytechnica Hungarica, February 2024, Vol.21, No.2., pp 187-202. ISSN 1785-8860

[Ma 2023] Ma, P., et al. Filter- and Observer-Based Finite-Time Adaptive Fuzzy Control for Induction Motors Systems Considering Stochastic Disturbance and Load Variation. IEEE Transactions on Power Electronics, February 2023, Vol.38, No.2., pp 1599-1609. ISSN 0885-8993

[Mohanty 2023] Mohanty, A. K. and Perli, S. B. Fuzzy Based Optimal Network Reconfiguration of Distribution System with Electric Vehicle Charging Stations, Distributed Generation, and Shunt Capacitors. Advances in Electrical and Electronic Engineering, June 2023, Vol.21, No.2., pp 81-91. ISSN 1336-1376

[Mynar 2021] Mynar, Z., Vaclavek, P. and Blaha, P. Synchronous Reluctance Motor Parameter and State Estimation Using Extended Kalman Filter and Current Derivative Measurement. IEEE Transactions on Industrial Electronics, March 2021, Vol.68, No.3., pp 1972-1981. ISSN 0278-0046

[Ontiveros-Robles 2018] Ontiveros-Robles, E., Melin, P. and Castillo, O. Comparative analysis of noise robustness of type 2 fuzzy logic controllers. Kybernetika, February 2018, Vol. 54, No.1., pp 175-201. ISSN 0023-5954

[Perdukova 2023] Perdukova, D. and Fedor, P. Multi-Motor Drive Nonparametric Black-Box Fuzzy Model. MM Science Journal, June 2023, Vol.16, pp 6446-6452. ISSN 1803-1269

[Peterka 2020] Peterka, J., Nikitin, Y. R. and Bozek P. Diagnostics of Automated Technological Devices. MM Science Journal, October 2020, Vol.13, pp 4027-4034. ISSN 1803-1269

[Stender 2021] Stender, M., Wallscheid, O. and Bocker, J. Accurate Torque Control for Induction Motors by Utilizing a Globally Optimized Flux Observer. IEEE Transactions on Power Electronics, November 2021, Vol.36, No.11., pp 13261-13274. ISSN 0885-8993

[Tran 2017] Tran, T.C., et al. PID Speed Controller Optimization Using Online Genetic Algorithm for Induction Motor Drive. In: Duy, V., Dao, T., Kim, S., Tien, N., Zelinka, I., eds. Proceedings of the AETA 2016: Recent Advances in Electrical Engineering and Related Sciences, Busan, Korea, 8-10 December, 2016. Cham, Switzerland: Springer, Lecture Notes in Electrical Engineering, Vol. 415, pp 564-576. ISSN 1876-1100

[Vo 2023a] Vo, H. H. Sensorless Induction Motor Drive Using Modified Integral Sliding Mode Control-Based MRAS. Control Engineering and Applied Informatics, September 2023, Vol.25, No.3., pp 45-54. ISSN 1454-8658

[Vo 2023b] Vo, H. H. and Brandstetter, P. Modified Fuzzy Logic PI Speed Controller with Scheduling Boundaries of Integral Time Constant for PMSM Drive. Przeglad Elektrotechniczny, November 2023, Vol.99, No.11., pp 175-179. ISSN 0033-2097

CONTACTS:

Dung Quang Nguyen, M.Eng.
Modeling Evolutionary Algorithms Simulation and Artificial Intelligence, Faculty of Electrical and Electronics Engineering, Ton Duc Thang University
No. 19 Nguyen Huu Tho Street, Tan Phong Ward, District 7, Ho Chi Minh City, 72900, Vietnam
+84 28 3775 5028, nguyenquangdung@tdtu.edu.vn, 196217001@student.tdtu.edu.vn

Hau Huu Vo, Ph.D.
Modeling Evolutionary Algorithms Simulation and Artificial Intelligence, Faculty of Electrical and Electronics Engineering, Ton Duc Thang University
No. 19 Nguyen Huu Tho Street, Tan Phong Ward, District 7, Ho Chi Minh City, 72900, Vietnam
+84 28 3775 5028, vohuuhau@tdtu.edu.vn

prof. Ing. Pavel Brandstetter, CSc.
Department of Applied Electronics, Faculty of Electrical Engineering and Computer Science, VSB-Technical University of Ostrava
17. listopadu 15, 708 00 Ostrava, Czech Republic
+420 596 995 933, pavel.brandstetter@vsb.cz